ChemComm

COMMUNICATION

View Article Online
View Journal | View Issue

Cite this: *Chem. Commun.*, 2024, **60**, 10760

Received 31st July 2024,
Accepted 4th September 2024

DOI: 10.1039/d4cc03866e

rsc.li/chemcomm

Nitrogen fixation by alkali and alkaline earth metal hydrides assisted by plasma†

Han Wu,‡[ab] Kai Ma,‡[ab] Jiaqi Wen,[ab] Liang Yang,[c] Yeqin Guan,[ab] Qianru Wang,[ab] Wenbo Gao,[ab] Jianping Guo *[ab] and Ping Chen[ab]

The chemical behaviors of alkali and alkaline earth metal hydrides including LiH, KH, MgH_2, CaH_2, and BaH_2 under nitrogen plasma differ significantly from one another, exhibiting an ammonia production trend that contrasts with that observed under thermal conditions. A prominent feature of KH is its ability to facilitate plasma-assisted N_2 fixation without generating H_2 byproduct, showing high atomic economy in utilization of hydride ions for N_2 reduction.

Dinitrogen (N_2) fixation is not only of scientific significance but also plays a paramount role in preparation of ammonia (NH_3), which is a key raw molecule for producing nitrogen-based fertilizer and has been widely considered as an important energy or hydrogen carrier.[1] Currently, NH_3 is synthesized using the established and centralized Haber–Bosch process, which operates under harsh conditions (>673 K, >10 MPa) and is energy intensive. The reduction of energy loss and the development of medium for decentralized, distributed renewable energy storage have heightened the urgent need for sustainable ammonia synthesis approaches.[2] Significant efforts have been directed toward low-temperature thermal-catalytic, electro-chemical, photo-chemical, plasma-catalytic, and chemical looping ammonia synthesis methods.[3–7] And a number of new materials for nitrogen fixation have emerged.

Hydride (H^-)-containing materials, such as alkali and alkaline earth metal hydrides, transition metal hydrides and oxyhydrides, nitride-hydrides, and composite hydrides have shown great promise for N_2 fixation to NH_3.[8–13] For instance, alkali and alkaline earth hydrides such as LiH and BaH_2 can fix N_2 to form corresponding metal imides (Li_2NH and BaNH) upon heating to desired temperatures, accompanied by releasing H_2 (eqn (1)). The subsequent thermal hydrogenation of imides results in formation of NH_3 and regeneration of metal hydrides (eqn (2)).[11,14] NaH and KH, however, cannot fix N_2 under standard thermal conditions (Fig. S1, ESI†) due to the absence of thermodynamically stable imides.[15] We found unexpectedly, NaH is able to fix N_2 to form a surface $NaNH_2$ species with the assistance of plasma and the thermal hydrogenation of $NaNH_2$ to NH_3 occurs readily under low temperature, fulfilling a loop for ammonia production.[16] This plasma–thermal hybrid ammonia loop effectively prevents NH_3 from plasma-induced cracking, a challenging obstacle to overcome in plasma-catalytic ammonia synthesis.[17] Given the benefits of this hybrid chemical looping process for NH_3 synthesis, it is worthwhile to explore the potential of other alkali or alkaline earth hydrides, as well as those materials beyond hydrides. Herein, the interaction of a series of binary hydrides including LiH, KH, MgH_2, CaH_2, and BaH_2 with nitrogen plasma is investigated. Our findings reveal that their plasma-chemical responses under nitrogen plasma differ significantly from one another, exhibiting a trend that contrasts with that observed under normal thermal conditions. This study reveals the multi-facets of alkali and alkaline earth metal hydrides for N_2 fixation.

$$4LiH + N_2 \rightarrow 2Li_2NH + H_2 \quad (1)$$

$$Li_2NH + 2H_2 \rightarrow 2LiH + NH_3 \quad (2)$$

The chemical responses of a series of alkali and alkaline earth hydrides under argon or nitrogen plasma were investigated. Fig. S2 (ESI†) shows that, similar to NaH, all of the hydrides produce H_2 upon exposure to argon plasma, indicating the occurrence of dehydriding. Fig. 1a displays the time course of H_2 signals detected during the nitrogen plasma process. H_2 signals are also observed in LiH, CaH_2, and BaH_2 under nitrogen plasma. Taking LiH as an example, the intensity of the H_2 signal initially showed slow growth over the first 10 min and then gradually decreased over time. The H_2 signals declined quickly with the turn-off of the plasma. Differing significantly

[a] State Key Laboratory of Catalysis, Dalian Institute of Chemical Physics, Chinese Academy of Sciences, Dalian 116023, China. E-mail: guojianping@dicp.ac.cn
[b] Center of Materials Science and Optoelectronics Engineering, University of Chinese Academy of Sciences, Beijing 100049, China
[c] Key Laboratory of Chemical Lasers, Dalian Institute of Chemical Physics, Chinese Academy of Sciences, Dalian 116023, China

† Electronic supplementary information (ESI) available. See DOI: https://doi.org/10.1039/d4cc03866e

‡ These two authors contribute equally to this work.

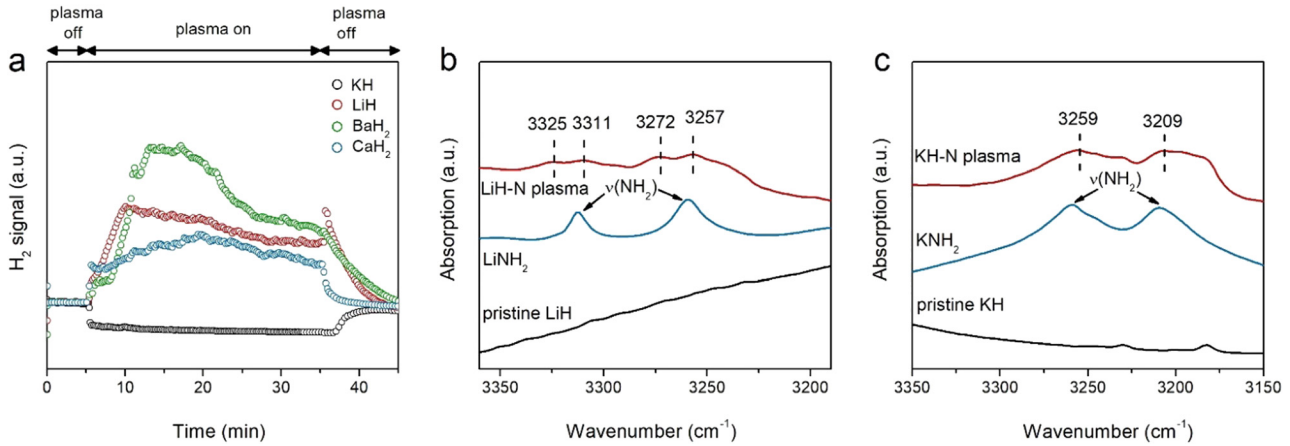

Fig. 1 (a) Time courses of H_2 MS signals (m/z = 2) for LiH, KH, CaH_2, and BaH_2 under nitrogen plasma. Voltage is 12 kV. Plasma power is *ca.* 8 W. FTIR spectra of LiH (b) and KH (c) collected after nitrogen plasma treatment and reference LiH, KH, $LiNH_2$, and KNH_2 samples.

from these hydrides, although dehydriding of KH also takes place under argon plasma (Fig. S2, ESI†), there is essentially no H_2 formation from the KH sample under nitrogen plasma (Fig. 1a). The differing behaviors of KH under Ar and nitrogen plasmas suggest that N_2 fixation by KH is fundamentally different from that of other alkali or alkaline earth metal hydrides.

Although they show different time courses of H_2 signals under argon or nitrogen plasma, it is difficult to ascertain whether N_2 fixation occurs based solely on the phenomenon of H_2 formation. Therefore, the solid products after nitrogen plasma treatment were subjected to XRD and FTIR characterization. As shown in Fig. S3 (ESI†), the phase structures of LiH and CaH_2 become amorphous after nitrogen plasma treatment, while the structure of KH remains largely unchanged although the intensity of the diffraction peaks significantly weaken. SEM images (Fig. S4, ESI†) show that, the morphology of samples collected after nitrogen plasma treatments remained unchanged, suggesting it is only the (sub)surface of hydrides that is involved in the N_2 fixation process. Fig. 1b, c and Fig. S5 (ESI†) show the FTIR spectra of different hydride samples after nitrogen plasma. LiH and KH exhibit prominent N–H vibrations, while there are no significant N–H vibrations on CaH_2 and BaH_2. Specifically, several bands centered around 3325, 3311, 3272, and 3257 cm^{-1} are observed for the LiH sample, which could be assigned as the asymmetric and symmetric stretch vibrations of NH_2^- species (ν_{NH_2}) of $LiNH_2$, respectively. For KH, two observable bands centered around 3255 and 3206 cm^{-1} are clearly seen, which can be attributed to the surface KNH_2 species (3259 and 3209 cm^{-1}).

The presence of nitrogen species on the surfaces of alkali or alkaline earth metal hydrides after nitrogen plasma can be further verified and quantified by measuring the NH_3 produced when heated in a H_2 flow. Fig. 2a presents the temperature-programmed hydrogenation (TPH) profile for the KH powder pretreated under nitrogen plasma at 12 kV. The formation of NH_3 was monitored by using an on-line mass spectrometer and quantified by using a conductivity meter. It is clearly seen that NH_3 evolves in the temperature range of 100–350 °C with two peaks around 160 and 220 °C. The amount of fixed N is determined to be *ca.* 27.4 μmol and the conversion of KH could

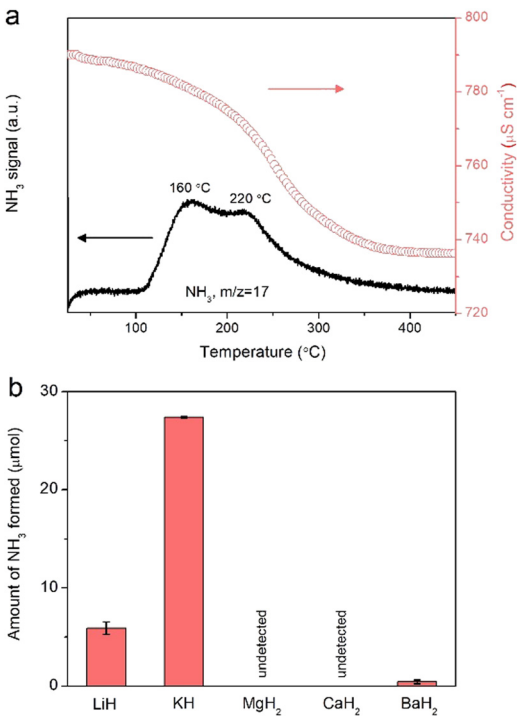

Fig. 2 (a) Temperature-programmed hydrogenation (TPH) profiles of NH_3 signal (m/z = 17) and conductivity decrease during the hydrogenation of the nitrogen plasma-treated KH sample. Sample mass is 30 mg. P_{H_2} is 1 bar. H_2 flow rate is 30 mL min^{-1}. (b) The amounts of fixed N in metal hydrides determined through TPH measurements. Voltage is 12 kV. Sample mass for LiH is 10 mg, and the others are 30 mg.

be estimated to 3.7%, suggesting that the N_2 fixation occurs mainly at the (sub)surface of KH. XRD pattern shows that the phase structure of the KH sample was not changed (Fig. S6, ESI†). H_2-TPR profiles for LiH and BaH_2 samples are shown in Fig. S7 (ESI†) and the amounts of produced ammonia are shown in Fig. 2b. The amounts of fixed N in LiH and BaH_2 are 5.9 and 0.45 μmol, respectively, while negligible amounts of NH_3 were obtained from the hydrogenation of plasma-treated

MgH_2 and CaH_2 samples. Since some nitrogen species may not react with H_2 below 450 °C, an alternative method for NH_3 measurement, *i.e.*, hydrolysis of these samples using water vapor was also studied under room temperature. The hydrolysis of the MgH_2, CaH_2, and BaH_2 samples after nitrogen plasma treatment produces a measurable amount of NH_3. The amounts of fixed nitrogen were determined to 1.1, 2.7, and 0.6 μmol by using hydrolysis method, respectively (Fig. S8, ESI†). Based on these results, it can be concluded that LiH, KH, MgH_2, CaH_2, and BaH_2 are able to fix N_2 under nitrogen plasma, but the amounts and fate of the fixed N vary significantly. We suppose the varying capacities of hydrides for plasma nitrogen fixation may be related to their different lattice energies. As shown in Table S1 (ESI†), alkali hydrides have much smaller lattice energies compared to their alkaline earth counterparts,[18] which may facilitate the dehydriding and accommodation of nitrogen in hydrides.

It has been reported that N_2 fixation by LiH, CaH_2, and BaH_2 produces H_2 and the corresponding metal imides under thermal conditions (eqn (1)). Under nitrogen plasma, NaH can also fix N_2 to form $NaNH_2$ and H_2.[16] The phenomenon of H_2 formation has also been observed in the nitrogen fixation processes mediated by some molecular transition metal hydrido complexes and nitrogenase enzymes, increasing energy consumption.[19–21] The pathways of reductive elimination of H_2 ($2H^-$ leading to H_2 and 2e, which then reduce N_2), and reductive protonation (H^- leading to H^+ and 2e) have been proposed to account for the formation of H_2 by-product and N–H bond during nitrogen fixation process, respectively. The interaction of KH with nitrogen plasma is, however, fundamentally different: KH fixes N_2 to form NH_2 species without releasing H_2 under plasma conditions. Therefore, majority of hydride ions in KH can be used for N_2 reduction and N–H bond formation, which is virtually more efficient for utilization of hydride than those of LiH, NaH, CaH_2, and BaH_2. There are two possible routes for N–H bond formation. For one thing, the hydrides act as electron sources for N_2 reduction through the reductive elimination of H atoms (H^- leading to H and e), which then undergo further reductive protonation to form NH_2 species instead of generating H_2 (eqn (3)). On the other hand, the impact of energetic particles in plasma leads to the dehydriding of KH to form K and H_2 as demonstrated by H_2 formation under argon plasma (Fig. S2, ESI†) and a strong and symmetrical EPR signal (Fig. S9, ESI†). H_2 then easily reacts with reactive N species in plasma forming gaseous NH_3. NH_3 may react with K through two possible pathways, *i.e.*, to form KNH_2 and H_2 (eqn (4)), or to form KNH_2 and KH (eqn (5)). Noted there is no H_2 formation in the latter pathway. Fig. 3 depicts the free energy changes (ΔG) of these two reaction pathways as a function of temperature. It is seen that the reaction between K and NH_3 to form KNH_2 and KH is thermodynamically more favorable than the formation of KNH_2 and H_2 under room temperature. It is known that KNH_2 and KH can form a amide-hydride $K(NH_2)_x(H)_{1-x}$ solid solution,[22] which will further promote the reaction (4). While for the reaction of Na and NH_3, the formation of $NaNH_2$ and H_2 is more favorable under room temperature (Fig. S10, ESI†).

$$4KH + N_2 \rightarrow 2KNH_2 + 2K \quad (3)$$

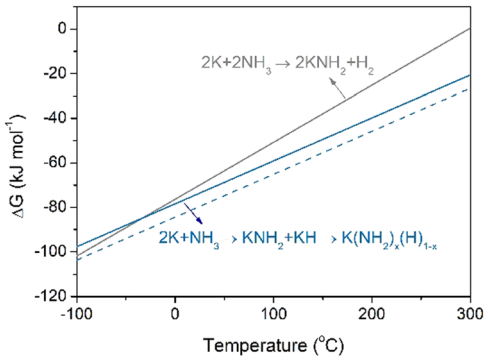

Fig. 3 Temperature dependences of ΔG for reactions of K and NH_3 to form different products. The enthalpies of KH and KNH_2 are taken from the literature.[15] The entropies of solids are not considered. The dashed line serves as a guide, illustrating that the formation of $K(NH_2)_x(H)_{1-x}$ solid solution is thermodynamically more favorable.

$$2K + 2NH_3 \rightarrow 2KNH_2 + H_2 \quad (4)$$

$$2K + NH_3 \rightarrow KNH_2 + KH \quad (5)$$

As demonstrated in previous sections, the synergy of plasma and alkali and alkaline earth metal hydrides enables N_2 fixation, and the following thermal hydrogenation of fixed N produces NH_3. The performance of plasma–thermal hybrid chemical looping ammonia synthesis (PCLAS) for these metal hydrides was thus evaluated. The PCLAS process is basically composed of two steps, *i.e.*, step I—plasma-driven nitrogen fixation in alkali or alkaline earth hydrides, and step II—thermal hydrogenation of the fixed nitrogen to NH_3 which was operated in a temperature-programmed heating mode. The averaged ammonia production rates over a series of hydride samples are presented in Fig. 4. Generally, the chemical looping ammonia production rate follows the order: KH > NaH > LiH > BaH_2, while MgH_2 and CaH_2 produce negligible amounts of NH_3 under the same reaction condition. The NH_3

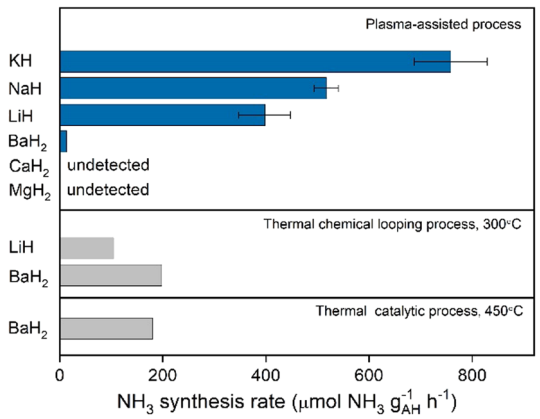

Fig. 4 Chemical looping ammonia production rates of a series of AH samples. The voltage is 12 kV. Error bars represent the standard deviation from three independent measurements. The data of thermal looping and catalytic rates are taken from ref. 11 and 23 and the data of NaH is taken from ref. 16.

production rate increases with the increasing of the applied voltage (Fig. S11, ESI†). The highest ammonia production rate was obtained over an applied voltage of 12 kV. Under a voltage of 12 kV, the rates of loops mediated by KH, LiH, and BaH_2 are 758, 398, and 13 μmol g^{-1} h^{-1}, respectively. And the NH_3 production rate of KH is slightly higher than that reported on NaH (*ca.* 550 μmol g^{-1} h^{-1}). This trend is inversely proportional to their lattice energies as shown in Table S1 (ESI†). The ammonia production rates of PCLAS are also compared with some reported data of conventional thermal chemical looping or thermal-catalytic process mediated by hydrides. As shown in Fig. 4, the KH-mediated PCLAS produces NH_3 at a rate that is *ca.* 3–7 times of the thermal-CL mediated by LiH and BaH_2 samples conducted at 300 °C and the thermal-catalytic rate of BaH_2 at 450 °C.

In summary, the interaction of a series of alkali and alkaline earth hydrides including LiH, KH, MgH_2, CaH_2, and BaH_2 with nitrogen plasma has been studied. They show quite different behaviors under nitrogen plasma or thermal conditions. Specifically, LiH can mediate both nitrogen fixation, whether through nitrogen plasma or heating, as well as the subsequent thermal hydrogenation to produce NH_3, thus completing an ammonia loop. KH together with NaH can only facilitate nitrogen fixation under plasma conditions, while the thermal hydrogenation of fixed nitrogen to NH_3 is easier at low temperatures. MgH_2, CaH_2, and BaH_2 can all fix N_2 under thermal conditions; however, they do not effectively accommodate a significant amount of N atoms under nitrogen plasma conditions. Their different behaviors could be related to their different lattice energies. Among these binary hydrides, KH is very special because it does not release H_2 during N_2 fixation process. Searching for other ternary or multi-nary alkali or alkaline earth metal hydrides to manipulate their chemical properties under plasma is worthy of future studies.

The authors are grateful for financial support from the National Key R&D Program of China (2021YFB4000400), National Natural Science Foundation of China (Grant No. 21988101, 22109158, and 11905223), and Youth Innovation Promotion Association CAS (No. Y2022060 and 2022180).

Data availability

The data are available from the corresponding author on reasonable request.

Conflicts of interest

There are no conflicts to declare.

References

1 W. I. F. David, G. D. Agnew, R. Bañares-Alcántara, J. Barth, J. B. Hansen, P. Bréquigny, M. de Joannon, S. F. Stott, C. F. Stott, A. Guati-Rojo, M. Hatzell, D. R. Macfarlane, J. W. Makepeace, E. Mastorakos, F. Mauss, A. Medford, C. Mounaim-Rousselle, D. A. Nowicki, M. A. Picciani, R. S. Postma, K. H. R. Rouwenhorst, P. Sabia, N. Salmon, A. N. Simonov, C. Smith, L. Torrente-Murciano and A. Valera-Medina, *J. Phys.: Energy*, 2024, **6**, e021501.
2 F. Chang, W. B. Gao, J. P. Guo and P. Chen, *Adv. Mater.*, 2021, **33**, e2005721.
3 T. N. Ye, S. W. Park, Y. F. Lu, J. Li, M. Sasase, M. Kitano, T. Tada and H. Hosono, *Nature*, 2020, **583**, 391–395.
4 B. H. R. Suryanto, K. Matuszek, J. Choi, R. Y. Hodgetts, H. L. Du, J. M. Bakker, C. S. M. Kang, P. V. Cherepanov, A. N. Simonov and D. R. MacFarlane, *Science*, 2021, **372**, 1187–1191.
5 X. B. Fu, J. B. Pedersen, Y. Y. Zhou, M. Saccoccio, S. F. Li, R. Salinas, K. T. Li, S. Z. Andersen, A. N. Xu, N. H. Deissler, J. B. V. Mygind, C. Wei, J. Kibsgaard, P. C. K. Vesborg, J. K. Norskov and I. Chorkendorff, *Science*, 2023, **379**, 707–712.
6 P. Mehta, P. Barboun, F. A. Herrera, J. Kim, P. Rumbach, D. B. Go, J. C. Hicks and W. F. Schneider, *Nat. Catal.*, 2018, **1**, 269–275.
7 J. G. Chen, R. M. Crooks, L. C. Seefeldt, K. L. Bren, R. M. Bullock, M. Y. Darensbourg, P. L. Holland, B. Hoffman, M. J. Janik, A. K. Jones, M. G. Kanatzidis, P. King, K. M. Lancaster, S. V. Lymar, P. Pfromm, W. F. Schneider and R. R. Schrock, *Science*, 2018, **360**, eaar6611.
8 P. K. Wang, F. Chang, W. B. Gao, J. P. Guo, G. T. Wu, T. He and P. Chen, *Nat. Chem.*, 2017, **9**, 64–70.
9 M. Kitano, Y. Inoue, H. Ishikawa, K. Yamagata, T. Nakao, T. Tada, S. Matsuishi, T. Yokoyama, M. Hara and H. Hosono, *Chem. Sci.*, 2016, **7**, 4036–4043.
10 Y. Kobayashi, Y. Tang, T. Kageyama, H. Yamashita, N. Masuda, S. Hosokawa and H. Kageyama, *J. Am. Chem. Soc.*, 2017, **139**, 18240–18246.
11 W. B. Gao, J. P. Guo, P. K. Wang, Q. R. Wang, F. Chang, Q. J. Pei, W. J. Zhang, L. Liu and P. Chen, *Nat. Energy*, 2018, **3**, 1067–1075.
12 Q. R. Wang, J. Pan, J. P. Guo, H. A. Hansen, H. Xie, L. Jiang, L. Hua, H. Y. Li, Y. Q. Guan, P. K. Wang, W. B. Gao, L. Liu, H. J. Cao, Z. T. Xiong, T. Vegge and P. Chen, *Nat. Catal.*, 2021, **4**, 959–967.
13 Y. Q. Guan, H. Wen, K. X. Cui, Q. R. Wang, W. B. Gao, Y. L. Cai, Z. B. Cheng, Q. J. Pei, Z. Li, H. J. Cao, T. He, J. P. Guo and P. Chen, *Nat. Chem.*, 2024, **16**, 373–379.
14 M. Ravi and J. W. Makepeace, *Chem. Commun.*, 2022, **58**, 6076–6079.
15 F. Chang, Y. Q. Guan, X. H. Chang, J. P. Guo, P. K. Wang, W. B. Gao, G. T. Wu, J. Zheng, X. G. Li and P. Chen, *J. Am. Chem. Soc.*, 2018, **140**, 14799–14806.
16 H. Wu, L. Yang, J. Wen, Y. Xu, Y. Cai, W. Gao, Q. Wang, Y. Guan, S. Feng, H. Cao, T. He, L. Liu, S. Zhang, J. Guo and P. Chen, *Adv. Energy Mater.*, 2023, **13**, e2300722.
17 Y. L. Wang, W. J. Yang, S. S. Xu, S. F. Zhao, G. X. Chen, A. Weidenkaff, C. Hardacre, X. L. Fan, J. Huang and X. Tu, *J. Am. Chem. Soc.*, 2022, **144**, 12020–12031.
18 S. Harder, *Chem. Commun.*, 2012, **48**, 11165–11177.
19 T. Shima, S. W. Hu, G. Luo, X. H. Kang, Y. Luo and Z. M. Hou, *Science*, 2013, **340**, 1549–1552.
20 D. F. Harris, Z. Y. Yang, D. R. Dean, L. C. Seefeldt and B. M. Hoffman, *Biochemistry*, 2018, **57**, 5706–5714.
21 C. J. M. van der Ham, M. T. M. Koper and D. G. H. Hetterscheid, *Chem. Soc. Rev.*, 2014, **43**, 5183–5191.
22 A. Santoru, C. Pistidda, M. H. Sorby, M. R. Chierotti, S. Garroni, E. Pinatel, F. Karimi, H. J. Cao, N. Bergemann, T. T. Le, J. Puszkiel, R. Gobetto, M. Baricco, B. C. Hauback, T. Klassen and M. Dornheim, *Chem. Commun.*, 2016, **52**, 11760–11763.
23 Y. Q. Guan, C. W. Liu, Q. R. Wang, W. B. Gao, H. A. Hansen, J. P. Guo, T. Vegge and P. Chen, *Angew. Chem., Int. Ed.*, 2022, **61**, e202205805.